Sensors and Actuators B 256 (2018) 465–471

Contents lists available at ScienceDirect

Sensors and Actuators B: Chemical

journal homepage: www.elsevier.com/locate/snb

Research Paper

High-performance hydrogen sensing properties and sensing mechanism in Pd-coated *p*-type Si nanowire arrays

Jisun Baek[a,1], Byungjin Jang[a,1], Min Hyung Kim[a], Wonkung Kim[a], Jeongmin Kim[a], Hyun Jun Rim[a], Sera Shin[b], Taeyoon Lee[b], Sungmee Cho[a], Wooyoung Lee[a,*]

[a] Department of Materials Science and Engineering, Yonsei University, 262 Seongsanno, Seodaemun-gu, Seoul, 129-749, Republic of Korea
[b] School of Electrical and Electronic Engineering, Yonsei University, 50 Yonsei-Ro, Seodaemun-gu, Seoul, 03722, Republic of Korea

ARTICLE INFO

Article history:
Received 28 May 2017
Received in revised form 8 October 2017
Accepted 18 October 2017
Available online 18 October 2017

Keywords:
Pd
Si nanowire arrays
Hydrogen gas sensor
Schottky/Ohmic contact

ABSTRACT

We report on the H_2 sensing performance and sensing mechanism in Pd-coated *n*- and *p*-type Si nanowire (NW) arrays, which were fabricated by an aqueous electroless etching method and sputtering. We found that the resistance of the Pd-coated *n*-type Si NWs decreased from the base resistance, whereas that of the *p*-type Si NW arrays increased, upon exposure to H_2. The sensitivity ($S = 1700\%$ at 1% H_2) of Pd-coated *p*-type NW arrays was much greater than that of the *n*-type NW arrays ($S = 75\%$). Furthermore, we found that the dependency of the change in carrier density on H_2 concentration was significantly greater in *p*-type Si NW arrays, while it was negligible in the *n*-type NW arrays. A Schottky barrier was formed between the Pd and *n*-Si ($\phi_M > \phi_{SC}$) before exposure to H_2, which changed to an Ohmic contact ($\phi_M < \phi_{SC}$) after H_2 exposure. In contrast, an Ohmic contact was formed between the Pd and *p*-Si ($\phi_M > \phi_{SC}$) before exposure to H_2, which, after exposure, changed to a Schottky barrier ($\phi_M < \phi_{SC}$). Therefore, the *p*-type Si NW arrays were much more sensitive to H_2 than the *n*-type Si NW arrays.

1. Introduction

Nanostructured Si materials have the potential to revolutionize its application to chemical sensors [1,2], pressure sensors [3], solar cells [4], and microelectromechanical systems (MEMS) [3,5], due to the unique optical, electronic, and mechanical properties of Si. Furthermore, Si has distinct intrinsic characteristics which enable rapid diffusion and adsorption of the target gas molecules that enters into the interlayer spaces, resulting in an improved sensor performance. Therefore, Si is used to achieve a high surface area-to-volume ratio by forming one-dimensional (1D) structures such as nanowires (NWs) [6–8] and nanorods [9,10].

Metallic Pd is considered one of the best materials for detecting H_2 gas owing to its superior hydrogen solubility at room temperature, compared to that of other alternatives such as metal oxides [11]. During hydrogen dissolution, a chemisorption reaction occurs by the selective dissociative adsorption of H_2 molecules on the Pd surface, followed by the diffusion of H_2 molecules into the interstitial sites of Pd. Because of hydrogen dissolution, the resistance of the material changes due to the formation of Pd/H (α phase) and Pd hydride (β phase) [12,13].

Pd nanostructures have been widely studied as H_2 gas sensors in high performance sensing devices, which are based on the high surface-to-volume ratio of the sensing element such as a single NW [14], NWs [15], thin films [12,13], nanoclusters [16,17], and porous membranes [18]. Recent advances in the development of H_2 gas sensors based on Pd NWs have shown improved gas sensing performances in terms of sensitivity, detection limit, and response/recovery times in air [19–21]. In a previous work [22], we reported the enhanced H_2 gas sensing properties of Pd-coated *n*-type Si NW arrays fabricated for the first time by a simple combination of Si electroless etching and Pd sputtering. Based on the concept of Pd-coated aligned Si NW arrays for the detection of H_2 [22], additional developments in vertical NW sensors were reported, not only for hydrogen sensing [23,24] but also for other applications such as NO_2 sensing [25], pH sensing [26], and the switching of water-adhesive properties [27].

Here, we report an advanced approach for H_2 gas sensing using Pd-coated *n*- and *p*-type Si NW arrays and a sensing mechanism that

* Corresponding author.
E-mail address: wooyoung@yonsei.ac.kr (W. Lee).
[1] These authors contributed equally to this work.

https://doi.org/10.1016/j.snb.2017.10.109
0925-4005/

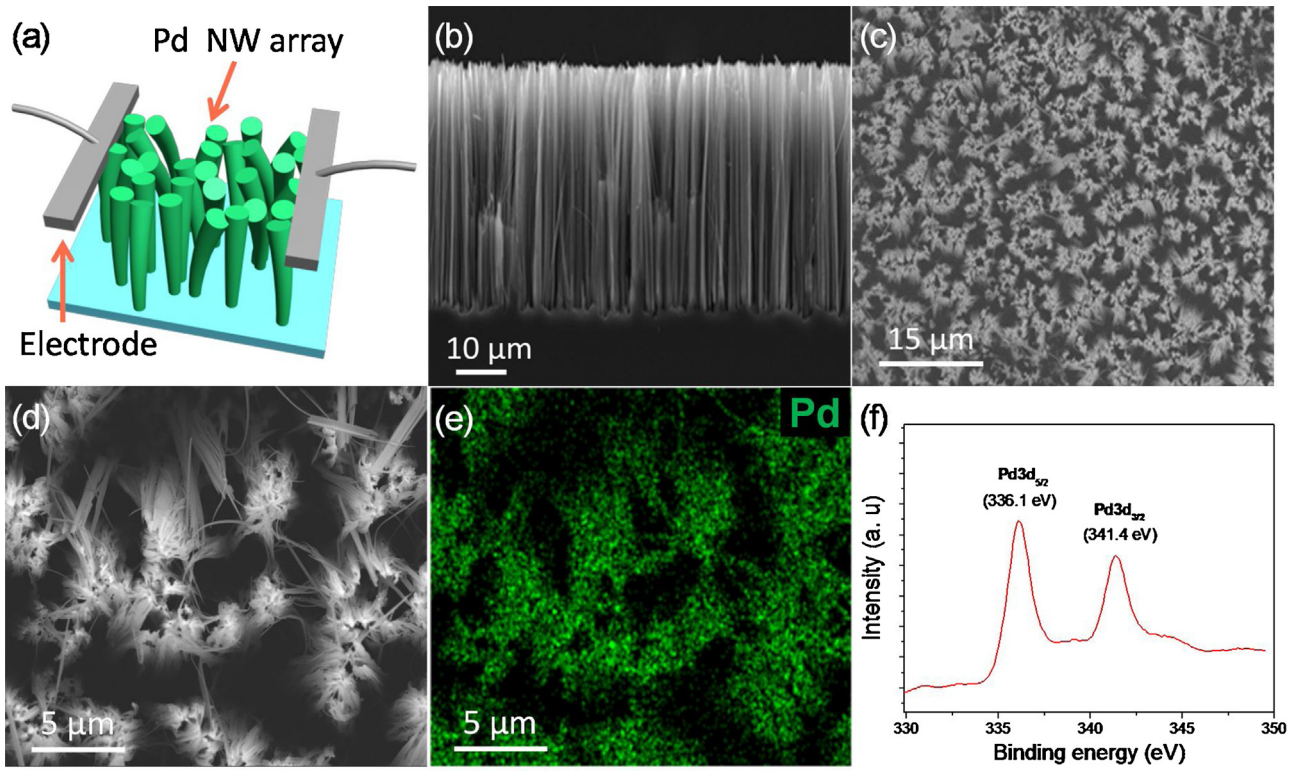

Fig. 1. (a) Schematic of a sensor device; (b) cross-sectional, (c) top view, (d) magnified top view SEM image of Pd-coated Si NW arrays; (e) EDX mapping of the magnified top view SEM image; and (f) XPS of Pd-coated Si NW arrays.

is dependent on the carrier type of the Si NWs. The newly proposed *p*-type Si NW arrays show an extremely enhanced H_2 sensitivity (S = 1700% at 10,000 ppm H_2), which is higher than that of the *n*-type Si NW arrays (S = 75% at 10,000 ppm H_2) by a factor of 23. The underlying sensing mechanism of the *n*- and *p*-type Pd-coated Si NW arrays is based on the change in their carrier concentrations due to the formation of Pd hydride (PdH_x) upon exposure to H_2. We discuss the hydrogen sensing mechanism of the Pd-coated Si NW arrays based on the semiconductor type (*n*- and *p*-type) in more detail in later sections.

2. Experiment

2.1. Fabrication of Pd-coated NW arrays

Vertically aligned Si NW arrays were fabricated using a top-down aqueous electroless etching (AEE) method [22,27]. Four-inch, 500 ± 25-μm-thick *p*- (boron-doped) and *n*-type (phosphorus-doped) Si (100) wafers, each of which demonstrated resistivity values from 1 to 10 Ω-cm, were cleaned with acetone, methanol, and DI water for 20 min. In order to remove native oxide layers, the wafers were immersed in 50% HF and dipped in a mixed etching solution containing 0.03 M $AgNO_3$ and 6 M HF at 60 °C for 50 min. During the etching process, Ag^+ ions dissolved in the etching solution were randomly deposited on the Si surface by galvanic displacement [22,27]. After etching, the wafers were rinsed with a 30% HNO_3 aqueous solution and DI water to remove the undesired byproducts such as silver dendrites and particles. Finally, the fabricated Si NW arrays were dried in ambient atmosphere.

Pd was deposited on the Si NW arrays via an ultra-high vacuum DC magnetron sputtering system. The deposition was performed at 2.4×10^{-3} Torr in Ar at a flow rate of 34 sccm in a vacuum chamber with a base pressure of 4.7×10^{-8} Torr. The purity of the Pd target was 3 N, and the deposition rate of the Pd film at RT was ~3.7 Å/s at 20 W.

2.2. Characterization

The nanostructured assemblies of the Pd-coated Si NW arrays were characterized by field-emission scanning electron microscopy (FE-SEM; JSM-7001F, JEOL Ltd.) equipped with an energy dispersive X-ray spectrometer (FE-SEM-EDS; JEOL-7800F, JEOL Ltd.). The morphology of the Pd-coated single Si NW was investigated by the transmission electron microscopy (TEM; JEM-2100F, JEOL Ltd.).

2.3. Sensing measurements

The Pd-coated *p*- and *n*-type Si NW arrays were loaded onto a printed circuit board (PCB). Electrodes were constructed simply by pasting silver (P-100, Cans Inc.) on each top side of the Pd-coated Si NW arrays which is connected to the PCB by the identical paste. The performance of the NWs as H_2 sensors was assessed in a gas-testing chamber equipped with a mass flow controller (MFC). Hydrogen gas was supplied to the gas chamber at a constant flow of 1000 sccm. The sensing properties of the H_2 sensor were measured by monitoring the change in the resistance using a source-measure unit (Keithley 236, Keithley Instruments Inc.) with a constant voltage supply of 0.1 V for a time interval of 1 s. The concentration of H_2 was fixed in the range 2–10,000 ppm in air.

2.4. Hall measurements

The Hall measurements were also carried out using samples of the same structure as the H_2 sensing measurements on the PCB. The in-plane constant current (*x*-direction) of 5.00×10^{-4} A was applied through the silver paste electrodes used in the H_2 measurements

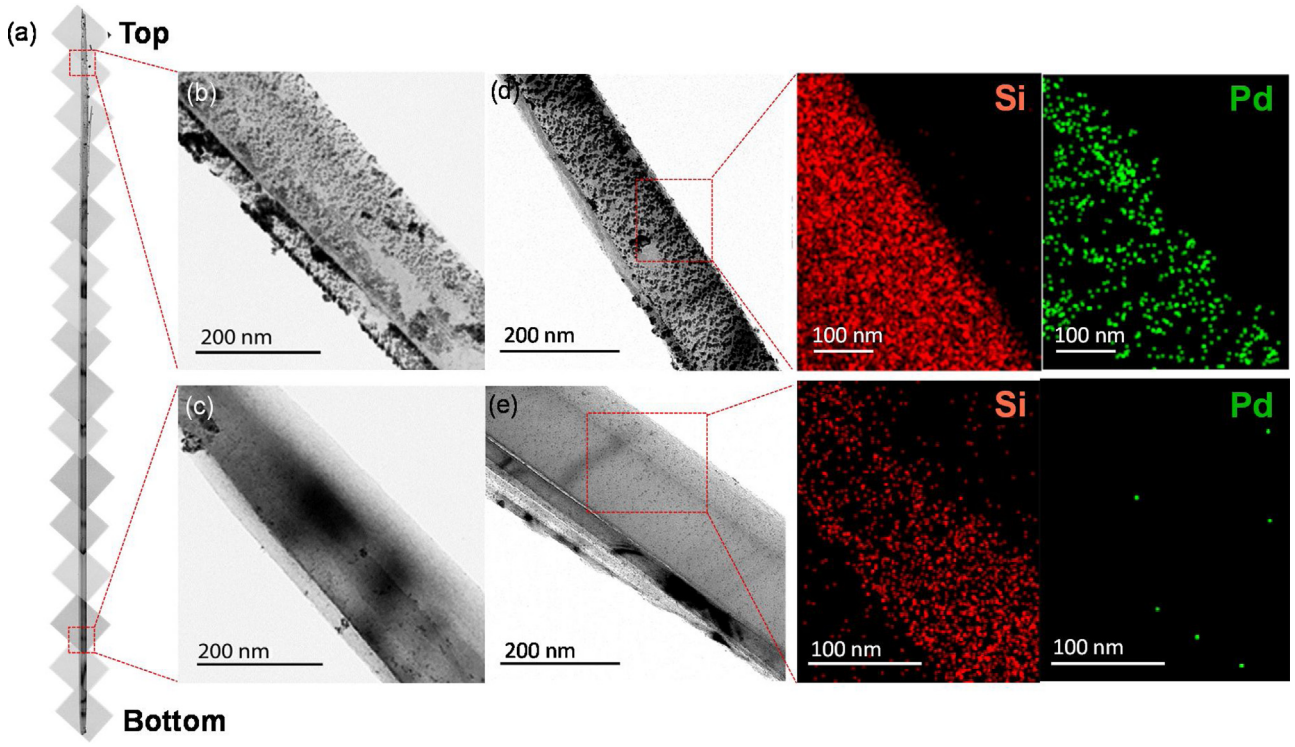

Fig. 2. (a) TEM images of a single Pd-coated Si NW. Magnified TEM images of (b) top and (c) bottom regions of the Pd-coated Si NW arrays. EDX mapping of (d) top and (e) bottom regions of the Pd-coated Si NW arrays.

using a current source meter (Keithley 236). The magnetic field (z-direction) along the out of plane direction was swept from −1 to 1T. For the Hall voltage measurement (y-direction), two additional electrodes were constructed using the silver paste and silver wires perpendicular to the current direction in-plane and the voltage difference were measured using a nano-voltmeter (Keithley 2182). A homemade acrylic chamber was used to control the H_2 concentration.

3. Results and discussion

Fig. 1(a–f) shows a schematic of the sensor device, the cross-sectional, top view, and magnified top view SEM images of the Pd-coated Si NW arrays, energy dispersive X-ray (EDX) mapping of the plane-view SEM image, and X-ray photoelectron spectroscopy (XPS) spectrum of the Pd-coated Si NW arrays, respectively. The schematic in Fig. 1(a) shows a sensor device with two electrodes on the Pd-coated Si NW arrays. The actual size of the sensor device is 1 cm (L) × 1 cm (W) × 500 μm (H). The Pd/Si NW arrays were bundled at their tips and formed local clusters due to the capillary force of the liquid during the drying process of the Si NW arrays [27]. The distance between the adjacent Pd/Si NW clusters ranged from 1 to 5 μm, whereas the inter-wire distance in a Pd/Si NW cluster was estimated to be in the range of sub-nm to a few nm [27].

The optimal condition for the fabrication of Si NW arrays was obtained by spatially controlling the Si NW growth by employing different etching times and compositional ratios of $AgNO_3$ and HF in the etching solution. As shown in the cross-sectional SEM image in Fig. 1(b), the average height of Si NWs is 30 μm, which readily resulted from an optimum $AgNO_3$:HF ratio of 0.03 M. The magnified SEM image in Fig. 1(d) shows an aggregation of individual Si NWs, highly perpendicular to the Si substrate. EDX mapping shown in Fig. 1(e) reveals the well prevalent regions in either Si or Pd, and shows that Pd displays a "shadow effect" wherein the green color is clearly visible. Due to the isotropic characteristic of the sputtering system, sputtered Pd atoms are shadowed by the previously formed Si NWs which prevent the atoms from reaching particular areas on the substrate. Therefore, the Pd nanoparticles are conformally coated on the Si NWs and induce a rough sidewall surface. EDX mapping reveals that Pd is deposited on the entire top surface of the Si NWs, with some depositions on the sidewalls as well. The XPS result further confirms the existence of Pd on the Si NW arrays (Fig. 1(f)). The XPS spectrum of Pd displays binding energy peaks at 336.1 eV and 341.4 eV, corresponding to the electronic transitions of Pd_{3d5A} and Pd_{3d3A}, respectively. The 5.3 eV gap between Pd_{3d5A} and Pd_{3d3A} indicates the value of the separated spin-orbit doublet, which is similar to those reported in literatures [28,29].

Transmission electron microscopy (TEM) images and EDX mapping of an individual single Pd-coated Si NW are presented in Fig. 2. A single Pd-coated Si NW shows a uniform diameter of approximately 200 nm (Fig. 2(a)). A large number of Pd nanoparticles appear on the surface the top region of the Si NW (Fig. 2(b)). However, Pd nanoparticles are hardly observed in the bottom region of the Si NW (Fig. 2(c)) since the poor step coverage of the sputtering process prevented the flow of Pd atoms to the base of the Si NW. The distribution of Pd nanoparticles on the entire Si NW was observed from EDX mapping of the top and bottom regions of the Si NW, as shown in Fig. 2(d) and (e). The Pd nanoparticles are deposited mainly on the top and top- and mid-sidewall of the Si NW.

Fig. 3 shows the H_2 sensing performance of the Pd-coated Si NW arrays. Specifically, the real-time electrical resistances of both the n- and p-type Si NWs were measured for various H_2 concentrations (n: 10,000–5 ppm, p: 10,000–2 ppm) in air at room temperature. The resistance of the Pd-coated n-type Si NWs decreased from the base resistance of 180 kΩ, whereas the resistance of the p-type Si NW arrays increased from 50 kΩ, for specific H_2 concentrations (Fig. 3(a)). We previously reported [22] that the resistance of the Pd-coated n-type NW arrays decreases in the presence of H_2 because the nearest NWs are connected by "*volume expansion*" of the Pd nanoparticles on their surfaces. Such "*volume expansion*" of Pd to

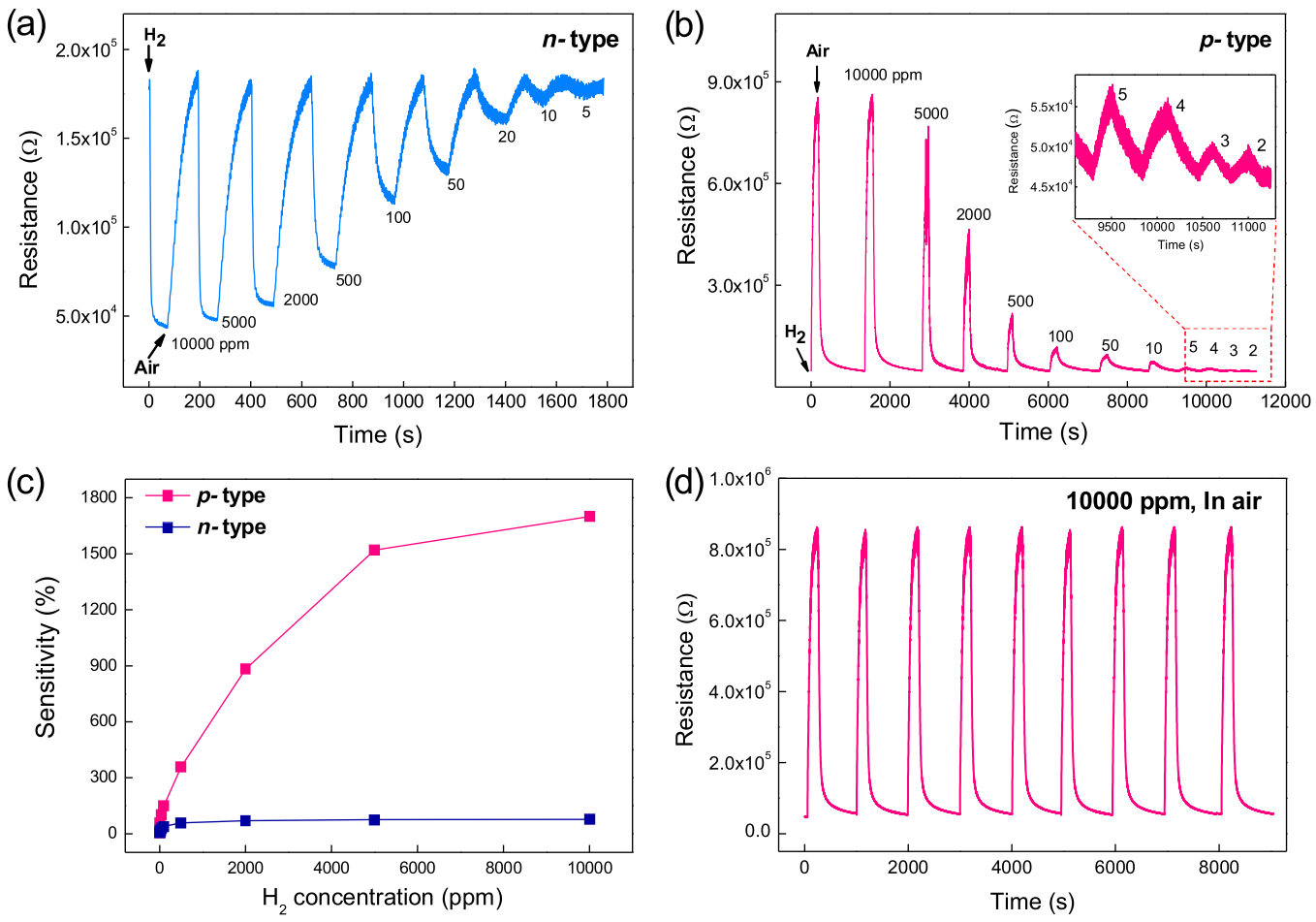

Fig. 3. Resistance vs. time plot of (a) *n*-type and (b) *p*-type Si NW arrays for various H_2 concentrations; (c) sensitivity as a function of H_2 concentration for *n*- and *p*-type Si NWs in air at room temperature; and (d) repeatability of the Pd-coated *p*-type Si NW arrays.

PdH_x may create additional carrier paths, thus decreasing the resistance [22]. However, we suspect that there is a limit to the "*volume expansion*" due to the low abundancy of Pd nanoparticles in the bottom region. Contrary to the *n*-type Si NW arrays, the resistance of the *p*-type Si NW arrays significantly increased when exposed to H_2 (see Fig. 2(b)). This implies that the "*volume expansion*" of PdH_x is not the main factor affecting the resistance of the Si NW arrays in the presence of H_2, at least for the *p*-type NW arrays. In order to clarify the sensing mechanism, we focused on the carrier transport in the *n*- and *p*-type Si NW arrays, which will be discussed in detail later.

The sensitivities as a function of H_2 concentration are shown in Fig. 3(c) for the *n*-type and *p*-type NW arrays. The sensitivity is defined as:

$$S = \frac{(R_g - R_a)}{R_a} \times 100, \quad (1)$$

where R_a and R_g are the resistances of the NW arrays before and after H_2 exposure in air, respectively. Interestingly, the *p*-type Si NW arrays showed extremely enhanced H_2 sensitivity ($S = 1700\%$ at 10,000 ppm H_2), which was higher than that of the *n*-type Si NW arrays ($S = 75\%$ at 10,000 ppm H_2) by a factor of 23. This indicates that the carrier type in Pd-coated Si NW arrays plays a crucial role in H_2 sensing. Moreover, the *p*-type Si NW arrays exhibited good repeatability in air, showing a reasonable response for the repeated 9 in/out cycles for 10,000 ppm H_2 (Fig. 3(d)).

A H_2 sensing mechanism based on the changes in resistance, which are opposite for the *n*- and *p*-type Si NW arrays, can be attributed to the interface effect of Pd/Si as depicted in Fig. 4. In the case of *n*-type Si NW arrays, the dissociation of hydrogen molecules into hydrogen atoms converts the coated Pd on Si NWs to PdH_x, which lowers the work function of Pd ($\phi_{Pd} > \phi_{PdHx}$), thereby facilitating the transfer of electrons from PdH_x to *n*-type Si NWs (Fig. 4(a)) [30]. In other words, when exposed to H_2, the resistance of the Pd-coated *n*-type Si NW arrays decreases, as shown in Fig. 4(b). However, when exposed to H_2, the formation of PdH_x in the *p*-type Si NW arrays lowers the work function of Pd ($\phi_{Pd} > \phi_{PdHx}$) and facilitates the transfer of electrons to the *p*-type Si NWs, which neutralizes the hole carriers (Fig. 4(c)). Thus, the resistance of the Pd-coated *p*-type Si NW arrays increases (Fig. 4(d)) [31].

The H_2 sensitivity of *p*-type Si NW arrays, which is significantly enhanced compared to that of *n*-type, can also be explained by the interface effect based on the change of work function. Since the work function of Pd ($\phi_{Pd} = 5.6$ eV) is larger than that of Si ($\phi_{n\text{-}Si} = 4.4$ and $\phi_{p\text{-}Si} = 4.9$ eV), a Schottky barrier is formed between Pd and *n*-Si ($\phi_M > \phi_{SC}$) (Fig. 5(a)) [32]. After exposure to H_2, an Ohmic contact ($\phi_M < \phi_{SC}$) is formed due to the reduction of work function owing to the formation of PdH_x (Fig. 5(b)) [32]. In contrast, an Ohmic contact is formed between the Pd and *p*-Si ($\phi_M > \phi_{SC}$) (Fig. 5(c)) [32,33], which, after exposure to H_2, changes to a Schottky barrier ($\phi_M < \phi_{SC}$) due to the reduction of work function owing to the formation of PdH_x (Fig. 5(d)) [32,33]. Since the Ohmic contact in the *p*-type Si NW arrays changes to a Schottky barrier upon exposure to H_2, the decrease in the work function of PdH_x with increasing H_2 concentration increase the height of the Schottky

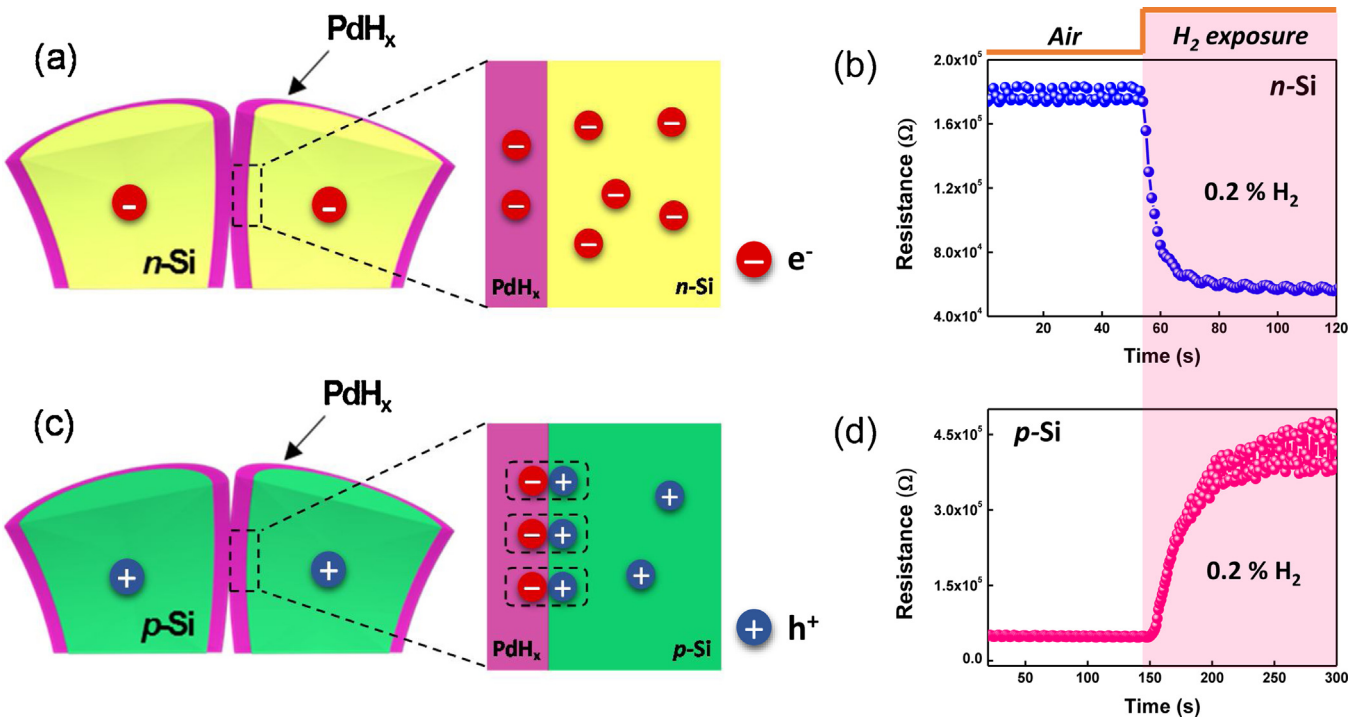

Fig. 4. Schematic illustration of H_2 sensing mechanisms in (a) *n*- and (c) *p*-type Pd-coated Si NW arrays based on carrier concentration. Resistance variation with time for 0.2% H_2 depending on the major carrier types in (b) *n*- and (d) *p*-type Pd-coated Si NW arrays.

barrier [32,33]. Thus, the resistance of the *p*-type Si NW arrays increases with increasing H_2 concentration. However, since the Schottky barrier in the *n*-type Si NW arrays changes to an Ohmic contact upon exposure to H_2, the interface effect of Pd/Si diminishes with increasing H_2 concentration. Consequently, the sensitivity of the Pd-coated *p*-type NW arrays is much higher than that of the *n*-type NW arrays. A native SiO_2 layer (~10 Å) in Pd/Si interface [34] serves as a diffusion barrier against palladium silicide (PdSi) formation while concurrently reducing the effect of Fermi level pinning [32]. If a SiO_2 layer is not formed on an *n*-/*p*-type Si NW, a schottky barrier forms between PdSi and a Si NW, resulting in no response to hydrogen gas [33]. It should be noted that a native SiO_2 layer is omitted between Pd and *n*-/*p*-type Si in the schematic diagram as shown in Fig. 5.

To validate the sensing mechanism, the changes of intrinsic properties in *n*- and *p*-type Si NW arrays were investigated with respect to the H_2 exposure by using the Hall measurement, as shown in Fig. 6. The Hall voltage is defined as:

$$V_H = \frac{IB}{ntq}, \tag{2}$$

where *I* is the current, *B* is the magnetic field, *n* is the number of charge carriers, *t* is thickness of the film, and *q* is the carrier charge (*e* for hole and −*e* for electron, *e* is the electronic charge). In typical conductors, the carrier density can be obtained with the slope of Hall voltage vs. magnetic field plot (V_H/B), according to Eq. (2). Although it is difficult to accurately define the thickness of the sample, in which the electrical conduction occurs, in this Pd-coated NW arrays, the change in the carrier density can be estimated by the absolute value of slope. In the *n*-type Si NW array, the absolute value of slope slightly decreases with the H_2 exposure as shown in Fig. 6(a), which indicates an increase of the carrier density (electrons). On the other hand, the *p*-type Si NW arrays showed increases of the slope with increasing H_2 concentration indicating decreases of carrier density (holes) (Fig. 6(b)). Moreover, the variation of slope in the *p*-type is more than one order magnitude larger than that of the *n*-type, which is good agreement with the H_2 sensing results. Furthermore, the noise level of Hall voltage increases as increasing H_2 concentration for the *p*-type NW, while the scattered Hall voltage is noticeable solely in air for the *n*-type. This noise is due to the increase in the contact resistance originating from the Schottky barrier at the Pd/Si interface, which is good agreement with the variation of interface explained above.

4. Conclusions

In summary, we have investigated the H_2 sensing performance of Pd-coated *n*- and *p*-type Si NW arrays, which were fabricated by an aqueous electroless etching method and sputtering. We found that the resistance of the Pd-coated *n*-type Si NWs decreased from the base resistance of 180 kΩ, whereas that of the *p*-type Si NW arrays increased from 50 kΩ, for 1% H_2. In addition, the *p*-type Si NW arrays showed ultra-high H_2 sensitivity (S = 1700% at 10,000 ppm H_2), which was higher than that of the *n*-type Si NW arrays (S = 75% at 10,000 ppm H_2) by a factor of 23. Moreover, upon exposure to H_2, the resistance of the Pd-coated *n*-type Si NW arrays decreased, while that of the Pd-coated *p*-type Si NW arrays increased. This is because the formation of PdH_x in the *p*-type Si NW arrays lowers the work function of Pd ($\phi_{Pd} > \phi_{PdHx}$) and results in the transferring of electrons to the *p*-type Si NWs, which neutralizes the hole carriers. Since the Schottky barrier in the *n*-type Si NW arrays changes to Ohmic contact when exposed to H_2, the interface effect of Pd/Si diminishes with increasing H_2 concentration. On the other hand, since the Ohmic contact changes to Schottky barrier in the *p*-type Si NW arrays when exposed to H_2, the decrease in the work function of PdH_x with increasing H_2 concentration increases the height of the Schottky barrier in the *p*-type Si NW arrays, thereby increasing its sensitivity. The variation of slope in Hall voltage vs. magnetic field was consistent with the interface effect according to the H_2 concentration in both types Si NW arrays. We demonstrated that

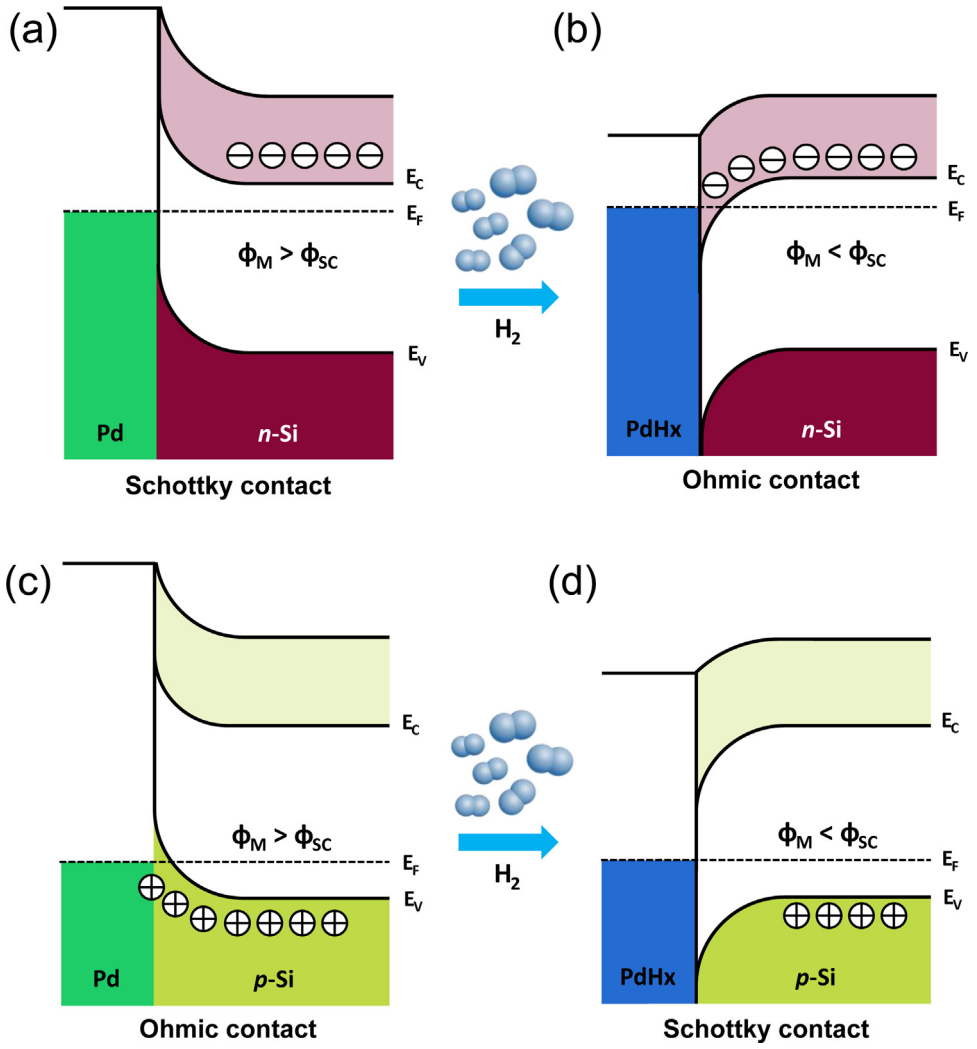

Fig. 5. Schematic illustration of the change in contact resistance at the metal (Pd)-semiconductor (Si) junction: (a) formation of Schottky barrier ($\phi_M > \phi_S$) in an *n*-type Si NW before the exposure of H_2, (b) formation of Ohmic contact ($\phi_M < \phi_S$) in the *n*-type Si NW after the exposure of H_2, (c) formation of Ohmic contact ($\phi_M > \phi_S$) in the *p*-type Si NW before the exposure of H_2, and (d) formation of Schottky barrier ($\phi_M < \phi_S$) in the *p*-type Si NW after the exposure of H_2.

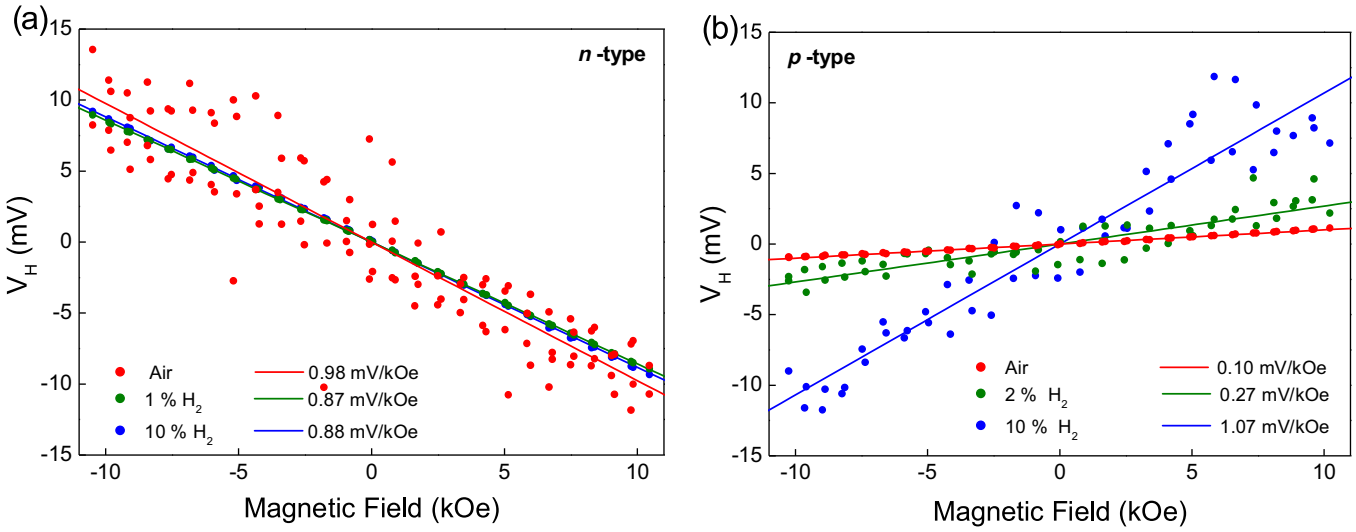

Fig. 6. Plot of Hall voltage vs. magnetic field revealing different carrier concentrations for various H_2 concentrations: (a) *n*- and (b) *p*-type Si NW arrays.

the sensitivity of Pd-coated *p*-type NW arrays is much higher than that of the *n*-type NW arrays.

Acknowledgments

This work was supported by the Korean government (MSIP) (2014R1A2A1A10053869), and the Priority Research Centers Program (2009-0093823) through the National Research Foundation of Korea (NRF).

References

[1] X.T. Zhou, J.Q. Hu, C.P. Li, D.D.D. Ma, C.S. Lee, S.T. Lee, Chem. Phys. Lett. 369 (1–2) (2003) 220–224.
[2] M. Gall, Sens. Actuators B: Chem. 4 (3–4) (1991) 533–538.
[3] J. Micromech. Microeng. 22 (2012) 055012.
[4] T. Stelzner, M. Pietsch, G. Andr, F. Falk, E. Ose, S. Christiansen, Nanotechnology 19 (2008) 295203–295206.
[5] R.R. Jivani, G.J. Lakhtaria, D.D. Patadiya, L.D. Patel, N.P. Jivani, B.P. Jhala, Saudi Pharam. J. 24 (1) (2016) 1–20.
[6] Y. Cui, Q. Wei, H.C. Park, K.C.M. Lieber, Science 293 (2001) 1289–1292.
[7] Z. Li, Y. Chen, X. Li, T.I. Kamins, K. Nauka, R.S. Williams, Nano Lett. 4 (2) (2004) 245–247.
[8] B.-C. Zhang, H. Wang, Y. Zhao, F. Li, X.-M. Ou, B.-Q. Sun, X.-H. Zhang, Nanoscale 8 (2016) 2123–2128.
[9] J. Fu, B. Park, G. Siragusa, L. Jones, R. Tripp, Y. Zhao, Y.-J. Cho, Nanotechnology 19 (15) (2008) 155502.
[10] S. Ma, M. Hu, P. Zeng, M. Li, W. Yan, Y. Qin, Sens. Actuators B: Chem. 192 (1) (2014) 341–349.
[11] F.A. Lewis, The Palladium Hydrogen System, Academic, New York, 1967.
[12] J. Lee, W.Y. Shim, E.Y. Lee, J.S. Noh, W.Y. Lee, Angew. Chem. Int. Ed. 50 (2011) 5301.
[13] E. Lee, J.M. Lee, J.H. Koo, W. Lee, T. Lee, Int. J. Hydrogen Energy 35 (2010) 6984.
[14] K.J. Jeon, M. Jeun, E. Lee, J.M. Lee, K.I. Lee, P. Allmen, W. Lee, Nanotechnology 19 (2009) 495501.
[15] F. Favier, E.C. Walter, M.P. Zach, T. Benter, R.M. Penner, Science 293 (2001) 2227.
[16] J. v. Lith, A. Lassesson, S.A. Brown, M. Schulze, J.G. Partridge, A. Ayesh, Appl. Phys. Lett. 91 (2007) 181910.
[17] Y.-S. Shim, D.H. Kim, H.Y. Jeong, Y.H. Kim, S.H. Nahm, C.-Y. Kang, J.-S. Kim, W. Lee, H.W. Jang, Sens. Actuators B: Chem. 213 (2015) 314–321.
[18] K. Luongo, A. Sine, S. Bhansali, Sens. Actuators B: Chem. 111–112 (2005) 125–129.
[19] F. Yang, S.-C. Kung, M. Cheng, J.C. Hemminger, R.M. Penner, ACS Nano 4 (2010) 5233.
[20] S. Cherevko, N. Kulyk, J. Fu, C.-H. Chung, Sens. Actuators B: Chem. 136 (2009) 388–391.
[21] X.Q. Zeng, M.L. Latimer, Z.L. Xiao, S. Panuganti, U. Welp, W.K. Kwok, T. Xu, Nano Lett. 11 (2011) 262–268.
[22] J.-S. Noh, H. Kim, B.S. Kim, E. Lee, H.H. Cho, W. Lee, J. Mater. Chem. 21 (2011) 15935–15939.
[23] B.-R. Huang, Y.-K. Yang, H.-L. Cheng, Nanotechnology 24 (47) (2013) 475502.
[24] Y. Qin, Y. Wang, Y. Liu, X. Zhang, Nanotechnology 27 (46) (2016) 465502.
[25] Y. Wang, M. Hu, Z. Wang, X. Liu, L. Yuah, Mater. Sci. Semicond. Process. 56 (2016) 307.
[26] J.-C. Lin, B.-R. Huang, Y.-K. Yang, Sens. Actuators B: Chem. 184 (31) (2013) 27–32.
[27] J. Seo, et al., Adv. Mater. 25 (2013) 4139–4144.
[28] Z. Wang, Z. Li, T. Jiang, X. Xu, C. Wang, ACS Appl. Mater. Interfaces 5 (2013) 2013–2021.
[29] S. Yang, J. Dong, Z. Yao, C. Shen, X. Shi, Y. Tian, S. Lin, X. Zhang, Sci. Rep. 4 (2014) 4501.
[30] B. Liu, D. Cai, Y. Liu, H. Li, C. Weng, G. Zeng, Q. Li, T. Wang, Nanoscale 5 (2013) 2505.
[31] J.L. Johnson, A. Behnam, S.J. Pearton, A. Ural, Adv. Mater. 22 (2010) 4877–4880.
[32] K. Skucha, Z. Fan, K. Jeon, A. Javey, B. Boser, Sens. Actuators B: Chem. 145 (2010) 232–238.
[33] P.F. Ruths, S. Ashok, S.J. Fonash, J.M. Ruths, IEEE Trans. Electron Devices 28 (9) (1981) 1003.
[34] M. Morita, T. Ohmi, E. Hasegawa, M. Kawakami, M. Ohwada, J. Appl. Phys. 68 (3) (1990) 1272.

Biographies

Jisun Baek was born in 1992 in Seoul, Republic of Korea. She received a BS degree in Department of Advanced Materials Engineering for Information & Electronics at KyungHee University in 2015. She is currently studying Hydrogen sensors based on Si nanowire as a step toward her M.S. degree in hydrogen sensor devices at Yonsei University.

Byungjin Jang was born in 1987 in Seoul, Republic of Korea. He received a BS degree in Material Science and Engineering at Yonsei University in 2011. He is currently studying MOTIFE sensors using Pd and gas sensors using various nanostructures as a step toward his Ph.D. degree at Yonsei University.

Min Hyung Kim was born in 1994 in Seoul, Republic of Korea. She received a BS degree in Material Science and Engineering at Yonsei University in 2017. She is currently studying Hydrogen sensors using various nanostructures as a step toward her MS. degree at Yonsei University.

Wonkyung Kim was born in 1976 in Mokpo, Republic of Korea. He received a B.E. in Material Science and Engineering at Yonsei University in 2007. He has been a High school teacher since 2002. He is currently studying MOTIFE sensors using Pd as a step toward his Ph.D. degree in hydrogen sensor devices at Yonsei University.

Jeongmin Kim obtained his BS degree in metallurgical engineering from the Yonsei University in 2008. He also earned his PhD degree under the supervision of Prof. Wooyoung Lee in the Department of Materials Science and Engineering at the Yonsei University include galvanomagnetic and thermoelectric transport properties of low dimensional materials. Throughout this time, his prime focus of research has been on studying and enhancing the thermoelectric performance of low-dimensional materials using nanowires based on bismuth.

Hyun Jun Rim was born in 1993 in Seoul, Republic of Korea. He received a BS degree in Renewable Energy Engineering at University of New South Wales in 2016. He is currently studying *p* and *n*-type thermoelectric materials such as magnesium and manganese silicide as a step toward his MS. degree at Yonsei University.

Sera Shin was born in 1991 in Boryeong, Republic of Korea. She received a B.E. in Electrical and Electronic Engineering at Yonsei University in 2013. She is currently studying surface engineering and fiber-based wearable electronics using various polymeric materials and metals as a step toward her Ph.D. degree at Yonsei University.

Taeyoon Lee is an associate professor of School of Electric and Electronic Engineering at Yonsei University in Korea. He received a BS degree in metallurgical engineering in 1995, a MS degree in metallurgical engineering from the Yonsei University in 1997. He received a Ph.D. degree in Materials Science & Engineering from University of Illinois at Urbana-Champaign in 2004. He is also Senior Fudan Fellow of Department of Material Science in Fudan University and the Convenor of International Electro technical Commission (IEC). In recent years, his research interests have centered on bio-inspired smart surface for biological and medical applications, textile-based electronics, and nanomaterials. He has received total 7 times company achievement awards in Intel California technology manufacturing and engineering due to contribution on the development of intellectual properties. He has authored and co-authored over 80 publications.

Sungmee Cho earned her Ph.D. degree in Electrical & Computer Engineering from Texas A&M University in 2011. She was a postdoc researcher in Materials Science and Engineering at Northwestern University in 2011–2012. She has been with Doosan Corporation as a researcher in 2003–2004 and Korea Institute Science Engineering (KIST) as a researcher in 2002–2003 and 2004–2005. Now she is a research professor in Creative Materials Division for BK21 PLUS program of Yonsei University. Her current research interests include Mg_2Si-based thermoelectric (TE) energy conversion, TE module joint, thin film hydrogen storage, hydrogen gas, solid oxide fuel cell (SOFC), and Li ion battery.

Wooyoung Lee is a professor of Department of Materials Science and Engineering, the director of Institute of Nanoscience and Nanotechnology at Yonsei University in Korea. He received a Ph.D. degree in physics from University of Cambridge, England in 2000. He has also taken part in the Korean Magnetics Society as the senior vice president of business and the Korean Sensors Society as the academic director. In recent years, his research interests have centered on smart nano-sensors and medical breath analyzers, thermoelectric materials and devices, and magnetic materials. He has received a number of awards in nano-related research areas and a Service Merit Medal (2008) from the Korea government due to contribution on the development of intellectual properties. He has authored and co-authored over 223 publications and has over 59 patents (domestic: 45, international: 14). He also edited a few of special books on nano-structured materials and devices.